ACS APPLIED MATERIALS & INTERFACES

Research Article

www.acsami.org

Multifunctional Nanoclay Hybrids of High Toughness, Thermal, and Barrier Performances

Houssine Sehaqui,*[,†,‡] Joby Kochumalayil,[‡] Andong Liu,[‡] Tanja Zimmermann,[†] and Lars A. Berglund[‡]

[†]Empa, Swiss Federal Laboratories for Materials Science and Technology, Applied Wood Materials Laboratory. Überlandstrasse 129, CH-8600, Dübendorf, Switzerland

[‡]Department of Fiber and Polymer Technology, Royal Institute of Technology, SE-100 44, Stockholm, Sweden.

Web-Enhanced Feature *Supporting Information*

ABSTRACT: To address brittleness of nanoclay hybrids of high inorganic content, ductile polymers (polyethylene oxide and hydroxyethyl cellulose) and montmorillonite (MTM) have been assembled into hybrid films using a water-based filtration process. Nacre-mimetic layered films resulted and were characterized by FE-SEM and XRD. Mechanical properties at ambient condition were studied by tensile test, while performance at elevated temperature and moisture conditions were evaluated by TGA, dynamic vapor sorption, and dynamic thermomechanical and hygromechanical analyses. Antiflammability and barrier properties against oxygen and water vapor were also investigated. Despite their high MTM content in the 60−85 wt % range, the hybrids exhibit remarkable ductility and a storage modulus above 2 GPa even in severe conditions (300°C or 94% RH). Moreover, they present fire-shielding property and are amongst the best oxygen and water vapor barrier hybrids reported in the literature. This study thus demonstrates nanostructure property advantages for synergistic effects in hybrids combining inexpensive, available, and environmentally benign constituents.

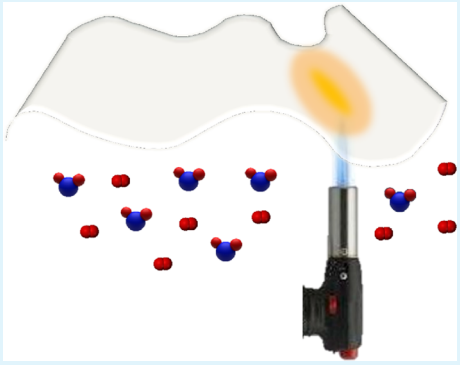

KEYWORDS: *hybrids, montmorillonite, nacre, ductile, gas barrier*

INTRODUCTION

In the quest for high performance, efficient, and multifunctional materials, the combination of organic and inorganic constituents intimately mixed at the nanoscale has proven to be a fruitful pathway. The large array of inorganic nanobuilding blocks available and advances made in soft inorganic chemistry processes significantly contributed to the development of hybrid materials and opened a wide range of promising application in many areas, such as optics, mechanics, environment, energy, and functional smart coatings.[1]

Polymer−clay nanocomposites are a class of hybrids generating great industrial and research interest. Clays show interesting features including natural abundance, platelet-like geometry with high aspect ratio and well-established intercalation chemistry. Their addition as a minor inorganic phase in polymer matrices results in nanocomposites exhibiting drastic improvements in strength,[2,3] modulus,[2,3] fire resistance;[4−7] and lower thermal expansion[8] and permeability to gases,[9,10] while retaining a high degree of optical transparency.[11,12−14] At high clay loading, dispersion within the organic matrix becomes challenging; poor control of the structure may result in clay aggregation, which leads to increased opacity and random platelet alignment that ultimately reduce performance (e.g., mechanical and barrier).[10]

On the other hand, natural composites such as nacre exhibit outstanding mechanical performance despite their high inorganic content (~95 wt %). In nacre, aragonite ($CaCO_3$) platelets are coated with a thin organic layer and ordered in parallel arrangement. The hard aragonite provides strength, while the soft organic layer dissipates viscoplastic deformation energy thus providing a high toughness to nacre, that is about 3 orders of magnitude higher than toughness of calcium carbonate, which is itself very brittle.[15]

Mimicking nacre structure is promising as it could lead to hybrids with enhanced performance compared to low volume fraction filled nanocomposites. This has been achieved by several strategies. Layer by layer (LbL) technique has been widely used to assemble oppositely charged inorganic and organic components into thin films with layered structure and high inorganic content (~70 wt %).[16−19] Nacre-structure mimicking by freeze casting is a multistep method where a layered template of the inorganic compound is first formed by unidirectional freezing of the corresponding suspension, this is followed by sublimation and template-filling with the organic component.[20,21] Clay platelets may be coated with a thin polymer layer then ordered into layered structures using doctor-blading[4,22] or simple paper making process.[22,23] Paper-making (i.e., vacuum filtration) is interesting as it may be adapted in continuous processes and results in superior clay platelet orientation parallel to the film surface in comparison to

Received: May 21, 2013
Accepted: July 9, 2013
Published: July 9, 2013

 © 2013 American Chemical Society

a conventional mixing and casting method.[23] The hybrids show outstanding mechanical,[16] barrier,[24,25] and antiflammability[22,23,25] properties that would not be possible through conventional nanocomposites.

In the present work, we extend the use of papermaking for the preparation of hybrids combining montmorillonite and ductile polymer matrices of high molar mass (polyethylene oxide and hydroxyethyl cellulose). Tough hybrids showing large improvement of thermal stability and high moisture barrier performance are obtained from water-based composites. Structural information of the hybrids is obtained by scanning electron microscopy, X-ray diffraction, and density measurement. Tensile mechanical properties are analysed in static and dynamic modes (temperature and humidity scans). Barrier properties against oxygen and water vapor are characterized at ambient and high moisture conditions, and flammability test is conducted. Comparison to other hybrids cited in the literature is provided.

MATERIALS AND METHODS

Hybrid and Reference Films Preparation. The clay used is a sodium montmorillonite (Cloisite Na+, Southern Clay Products) with a cation-exchange capacity (CEC) of 92 mequiv/100 g. The average size of the platelets is 110 nm as described by the manufacturer. Hydroxyethyl cellulose with average $M_v \approx 1\,300\,000$ g/mol and polyethylene oxide with a molecular weight of 600 000 g/mol were purchased from Sigma-Aldrich. A 0.8 wt % montmorillonite (MTM) suspension was prepared by dispersing 10 g of MTM in 1 L of deionized water under vigorous stirring (magnetic stirring overnight and ultra-turrax dispersion at 11 000 rpm for 30 minutes) followed by removal of sediments by gravitation. A 0.5 wt % aqueous solution of PEO or HEC was added to the MTM dispersion and the total concentration of the mixture was adjusted to 0.3 wt % by adding water. 200 ml of this mixture was stirred overnight, degassed, and then vacuum filtered on a glass filter funnel by using a 0.65 μm filter membrane (DVPP, Millipore). After vacuum filtration, any residual moisture was allowed to evaporate in air giving hybrid film of 72 mm in diameter. The variation of the organic and inorganic compounds proportion in the mixture resulted in hybrid films with different compositions. Note that some material loss occurred during vacuum filtration, and therefore the composition of the hybrids was determined by thermogravimetric analysis.

As reference, pure PEO and HEC films were prepared by casting a 0.3 wt % aqueous solution of the polymer into a petri dish and allowing water to evaporate at room temperature.

Field-Emission Scanning Electron Microscopy (FE-SEM). To get some insights onto the fracture mode of the hybrids, tensile fractured specimens were used for SEM observation. These were first dried in a desiccator overnight. Then the cross sections were observed with a Hitachi S-4800 scanning electron microscope equipped with a cold field emission electron source. Secondary electron detector was used for capturing images at 1 kV.

X-ray Diffraction (XRD). XRD patterns of pure MTM powder and hybrid films were recorded by an X'Pert Pro diffractometer (model PW 3040/60) at room temperature. The CuKα radiation source was operated with a tension of 45 kV and a current of 35 mA (λ = 1.5418 Å). Patterns were recorded by monitoring diffractions from 1° to 30°. An increment step of 0.05° and a rate of 1 step per 10 seconds were used.

Thermogravimetric Analysis (TGA). TGA was conducted to determine composition of the samples and to evaluate their thermal properties. This was performed on a Perkin-Elmer TGA7-thermal analyser from 25 to 800 °C with a heating rate of 10 °C min^{-1} under oxygen atmosphere with a flow rate of 50 mL min^{-1}. From TGA data, the temperature at maximum degradation rate (T_{max}) was taken as the temperature of the peak of the differential thermal analysis (DTA) plot. The temperature at the onset of thermal degradation was taken from the weight loss curve as the intersection of the horizontal plateau prior to thermal degradation and the subsequent downward slope. The inorganic content of the hybrids was taken as the weight fraction remaining at 800 °C.

Density of Hybrid Films. Density of the hybrids (ρ) was determined from their weight and their volume, the volume is taken as the product of the area and thickness of the film. The thickness was measured using a micrometer having an accuracy of 2 μm (Tesamaster, Long Island Indicator Service, Inc., U.S.A.). Porosity of the hybrids was calculated from their density by taking 1200, 1330, and 2860 kg m^{-3} as density for PEO, HEC, and MTM, respectively, using eq 1.

$$\text{porosity} = 1 - \frac{\rho}{\left(\frac{W_{MTM}}{\rho_{MTM}} + \frac{W_{pol}}{\rho_{pol}}\right)^{-1}} \quad (1)$$

Volume fraction of MTM excluding porosity was calculated using eq 2.

$$V_{MTM} = \frac{\rho_{pol} W_{MTM}}{\rho_{MTM} W_{pol} + \rho_{pol} W_{MTM}} \quad (2)$$

V and W refer to volume and weight fraction, respectively, and pol refers to polymer (HEC or PEO).

Tensile Mechanical Properties. Static tensile mechanical properties of hybrid films and reference polymers were characterized using an Instron universal material testing machine equipped with a 50 N load cell. The tests were performed at a relative humidity of 50% and temperature of 23 °C. Rectangular specimen strips of 50 mm in length, 5 mm in width, and a thickness of ~50 μm were tested at a strain rate of 10% min^{-1} and a gauge length of 30 mm. Three specimens were tested for each sample.

Thermomechanical Properties. Thermomechanical properties of hybrid films and reference polymers were determined in tension on a Q800 Dynamic Mechanical Analyser (TA Instruments, U.S.A.). Specimens used were 5 mm in width, and the distance between clamps was ~10 mm. Temperature scans were performed at a heating rate of 5° C min^{-1} and a frequency of 1 Hz from 25 °C to 300 °C in air.

Hygromechanical Properties. Hygromechanical properties of hybrid and reference polymer films were determined in tension on a Q800 Dynamic Mechanical Analyser (TA Instruments, U.S.A.) equipped with a humidity generator. Specimens used were 4 mm in width, and the distance between clamps was ca. 10 mm. The samples were first equilibrated at 25 °C and 0% RH for 2 h. Subsequently, relative humidity scan was performed from 0% RH to 94% RH at a rate of 1% RH min^{-1}, a frequency of 1 Hz and a deformation of 10 μm. Then, the samples were equilibrated at 94% RH for one hour under 1 Hz and 10 μm deformation.

Dynamic Vapour Sorption (DVS). Moisture sorption measurements were carried out with a VTI-SA+ dynamic vapor sorption analyser (TA-Instruments, New Castle, U.S.A.). A sample weighting ~10 mg was placed in the sample cup, and the precise weight of the sample compared to the reference was registered with a resolution of 0.1 μg, while the relative humidity (RH) surrounding the cups was controlled. The sample was first dried at 105 °C and 0% RH for two hours followed by equilibration at 23 °C. Then the humidity conditions were set to 50% and 85% RH, respectively. When the equilibrium was reached at each RH step, the moisture uptake of the sample with respect to its dry weight was obtained. Moisture uptake of the reference MTM was measured on the cloisite-Na$^+$ powder.

Water Vapor Barrier Properties. Water vapor permeability (WVP) of the films was measured by a VTI-SA+ dynamic vapor sorption analyser (TA-Instruments, New Castle, U.S.A.). Dried silica gel was placed in a small cup (10 mm in diameter and 10 mm in height), which was then sealed by a piece of the film. The sample was first dried at 60°C and 0% RH for one hour, followed by equilibration at 23°C. Then, the mass gain of the silica gel over time under 50% RH or 85% RH and 23 °C was measured. The WVP of the film was calculated from the steady state slope of the mass gain versus time according to the equations

$$\mathrm{WVP} = \frac{\mathrm{WVTR} \times \mathrm{thickness}}{\Delta P}$$

$$\Delta P = \frac{P_s(\mathrm{RH}_{out} - \mathrm{RH}_{in})}{100}$$

WVTR is the water vapor transmission rate, thickness refers to the thickness of the film, and P_s is the water vapor saturation pressure at 23 °C equal to 2800 Pa. RH refers to the relative humidity in percent and is RH_{out} = 50 or RH_{out} = 85 and RH_{in} = 0.

Oxygen Barrier Properties. Oxygen transmission rate (OTR) measurements at 23 °C and 80% RH were performed with Oxygen Permeation Analyser (Systech 8001, Systech Instruments Ltd., U.K.) equipped with a coulometric sensor following ASTM standard D3985-05. The test was performed on O_2 and N_2 flow using 100% oxygen as test gas. The active area of measurement was 5 cm^2. OTR measurements at 23°C and 50% RH were performed with a Mocon Oxtran 2/20 (Modern Controls, Minneapolis, MN) machine equipped with a coulometric sensor following ASTM standard D3985-05. The test gas was pure O_2 and the carrier gas was N_2 with 2% H_2. The active area of measurement was 5 cm^2.

RESULTS AND DISCUSSION

Hybrid Structure. In view of the preparation methods for nacre-mimetic hybrids, paper making is promising as it allows processing of large area hybrid films in fewer steps compared to layer by layer (LbL) or freeze casting methods.[22] Here, this method has been applied to prepare hybrid films ~50 micrometers thick combining MTM and a ductile polymer binder, namely, hydroxyethyl cellulose (HEC) or polyethylene oxide (PEO). Photographs of the hybrid films with 80 wt % MTM content are presented in Figure 1a. Advantage of vacuum filtration in terms of macroscopic flatness and smoothness of the films is apparent, similarly to what has been reported for other systems.[25,26] The films are yellowish yet translucent as a result of the nanosize dimension of the platelets and their limited aggregation in the films. While opacity is typical for microcomposites, high optical transparency may be achieved in thinner hybrid films[16] or in films with a lower inorganic content.[27,28] The hybrid films show high flexibility which is remarkable at such high inorganic content.

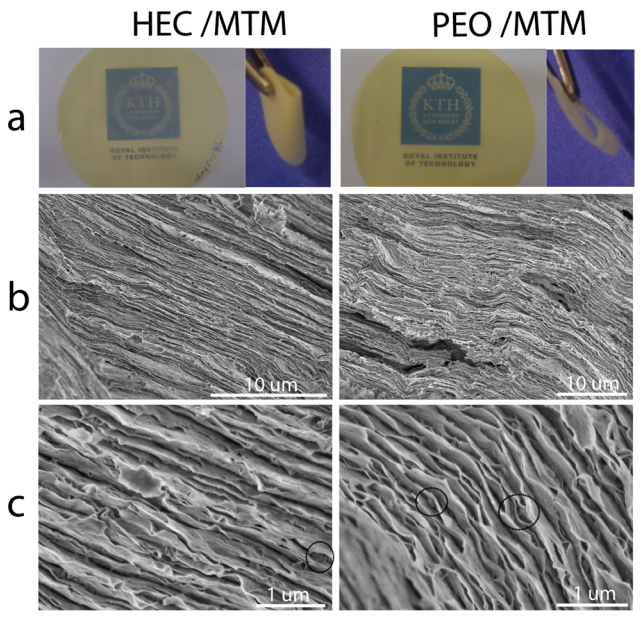

Figure 1. (a) Photographs of hybrid films on top of KTH logo showing optical translucency. Thickness of the films is ~50 μm. Images on the right show flexibility of hybrid films of ~4 × 4 cm^2. (b and c) Scanning electron micrographs showing cross sections of tensile fractured hybrid samples. Scale bars are 10 and 1 μm respectively. Circles in c show MTM tactoids. MTM content in the hybrids is 80 wt %.

Cross-section of tensile fractured samples was observed in FE-SEM. A layered structure typical for clay composites prepared by vacuum filtration[22,23,25] is observed throughout the thickness of the film (Figure 1b) with each layer being parallel to the film surface and occupying 100−200 nm. Such laminated structure has also been observed for cellulose nanopaper prepared by vacuum filtration[26,29] and may be associated with flocculation phenomena in the high concentration region close to the filtering membrane.[30] At higher magnification (Figure 1c), MTM tactoids of ~50 nm were observed (circles in Figure 1c, high resolution picture available in Supporting Information). These tactoids would correspond to 10−20 layers of polymer intercalated MTM platelets in a coplanar orientation[31] and are sandwiched between polymer-rich sheets. Signs of ductile fracture with plastic yielding of polymer-rich sheets are apparent in the fractured cross section as these sheets narrowed towards the fractured surface (Supporting Information).

The structure was further characterized by XRD. Diffractograms for pure MTM and for the hybrids are shown in Figure 2a. The pure MTM has a 2θ peak at 9 degrees corresponding to a d_{001} lattice spacing of 9.8 Å. The addition of PEO shifted the peak to 4.9 degrees indicating intercalation of PEO between clay platelets. The corresponding d_{001} is 18.1 Å indicating expansion of the clay galleries by ~8 Å. Identical intergallery spacing was reported in other PEO/MTM nanocomposites[32] and would correspond to intercalation of a double layer of PEO within Na-MTM galleries.[32,33] Interestingly, X-ray diffraction

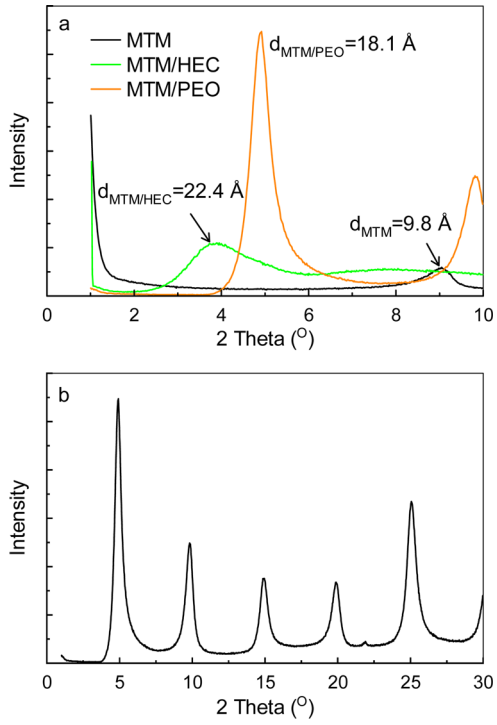

Figure 2. (a) X-ray diffractograms of pure MTM, and of PEO and HEC hybrids with 80 and 60 wt % MTM contents, respectively. (b) X-ray diffractogram of PEO hybrid between 0° and 30°.

dx.doi.org/10.1021/am401928d | ACS Appl. Mater. Interfaces 2013, 5, 7613−7620

patterns of PEO hybrid show regular d_{00l} reflections at multiples of 5° because of the regular and highly ordered lamellar arrangement of the PEO and nanoclay components (Figure 2b), as reported elsewhere.[32,34] X-ray diffractogram of MTM/HEC hybrid shows a broader peak at 3.9 degrees corresponding to a d_{001} lattice spacing of 22.4 Å and an expansion of the clay galleries by 12.6 Å (Figure 2a). PEO/MTM hybrid would have a more homogeneously ordered structure than HEC/MTM.

Structural information on the hybrids may also be obtained by density measurements. HEC and PEO hybrids with 72 and 77 wt % inorganic content have a density of 1810 and 1615 kg m^{-3}, respectively. This implies presence of porosity in the films (17% and 25%, respectively) as non-porous hybrids would have a density of ~2170 kg m^{-3}. A possible explanation is in the less efficient packing of the polymer chains between MTM galleries as has been suggested by Wu et al.[32] who found that the density of PEO in between MTM galleries is only 800 kg m^{-3}, thus lower than the 1200 kg m^{-3} of the bulk PEO polymer. Micrographs in Figure 1c suggest that pores may also be present in the interface of the polymer-rich and clay-rich regions. The size of these pores is far below the micrometer, while their shape is not known to us. Presence of porosity in the nanometer scale may be beneficial for a higher ductility of the hybrids as it offers room for polymer chain rearrangements.

Tensile Properties. Tensile stress–strain curves of the hybrids and neat polymers are presented in Figure 3, and

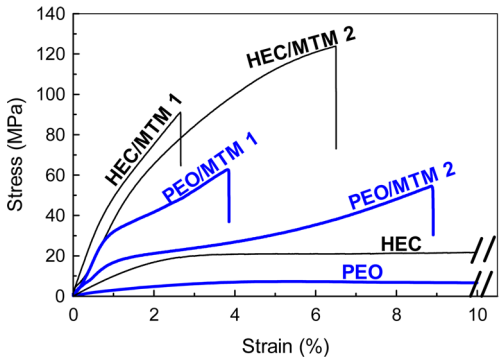

Figure 3. Uniaxial tensile stress-strain curves of MTM hybrids and neat polymer matrices. Hybrids composition is given in Table 1.

properties are summarized in Table 1. Ductility of the hybrids is noticeable as a clear and distinct plastic deformation zone in tensile stress-strain curves. The linear elastic deformation regime is occurring at low strain values below 1%. This is followed by a plastic deformation of the hybrid and finally ultimate failure of the sample. The strain to failure is then 2.7-8.6%. The plastic deformation zone with strain hardening is clearly seen particularly for the PEO hybrid in agreement with the ductile fracture observed in Figure 1c and is more pronounced (wider plastic deformation zone) for higher polymer content in the hybrid. Plastic deformation of the polymer would occur in between individual platelets and in the polymer-rich sheets, and the small size of the platelets/tactoids would limit macroscopic damages and brittle fracture of the hybrids.

Generally, mechanical properties of hybrids depend on a number of parameters such as inorganic content, nature of the inorganic/organic interface, platelets characteristics (geometry, surface area and distribution). Covalent bonding between the components may result in a very high stiffness and strength. Tensile modulus and strength reported for cross-linked thin films prepared by LbL are 106 GPa and 400 MPa, respectively, at the expense of a brittle fracture and a low strain to failure of only 0.33%.[16] In LbL, nanostructural control is realized by sequential adsorption of individual layers of inorganic and organic components, thin films instigate superior mechanical performance, and covalent bonding would promote platelet fracture mechanism. Our stiffness and strength data are much lower (2–5.8 GPa and 50–125 MPa respectively), while the ductility is far better. Presently, weaker bonds (hydrogen bonds and Van der Waal's interactions) are favored at the inorganic/organic interface and fracture rather occurs by platelet/tactoids pull-out resulting in the ductile behaviour observed.[49] The presence of a large number of platelets/tactoids in the fractured surface (Figure 1c and Supporting Information) may support the platelet pull-out mechanism suggested. Comparison to thicker samples is more relevant and shows that the present hybrids strength and stiffness data are comparable to data for cellulose nanofibers/MTM,[25] for CMC/MTM,[35] and for chitosan/MTM hybrids,[23] while they are lower than PVA/MTM[22] and a very recent CMC/MTM[36] hybrids, but again the strain-to-failure of the present materials (2.7–8.6%) is, to the best of our knowledge, higher than any other nacre-type hybrid with similar inorganic content and thickness (that is usually below 2%).[22,23,25,35–37] Even with a tough cellulose nanofibers matrix, the hybrids strain-to-failure is around 2%.[25] Thus, most distinctive features of the present hybrids are high ductility at relatively high strength resulting in exceptional toughness (work to fracture equal to the area under stress-strain curve).

Compared to neat polymer matrices, strength and stiffness data of the hybrids are increased by several times. Note that neat polymers have high strain to failure (Table 1), so that in combination with the platelets, they impart ductility to the hybrids through interlayer plastic deformation mechanisms, similar to what has been reported for cellulosic nanocomposites with a ductile HEC polymer matrix.[38,39]

Table 1. Tensile Mechanical Properties of MTM Hybrids and Neat Polymer Matrices[a]

sample	W_{pol}/W_{MTM}	V_{pol}/V_{MTM}	modulus (GPa)	strength (MPa)	strain-to-failure (%)
HEC	100/0	100/0	1.0 (0.2)	41 (7)	37 (4.4)
HEC/MTM 1	17/83	30/70	5.8 (0.6)	89 (7)	2.7 (0.2)
HEC/MTM 2	40/60	59/41	3.7 (0.8)	125 (7)	6.8 (1.1)
PEO	100/0	100/0	0.32 (0.06)	7.2 (0.4)	>100%
PEO/MTM 1	15/85	30/70	5.1 (0.4)	59 (7)	3.6 (0.5)
PEO/MTM 2	24/76	43/57	2.0 (0.1)	49 (8)	8.6 (0.9)

[a]Values in parentheses represent standard deviations. *W* and *V* refer to weight and volume fraction, respectively. pol refers to the polymer (HEC or PEO). Strength refers to the stress at break.

Thermogravimetric Analysis. Thermal degradation of the hybrids has been assessed by thermogravimetric analysis (TGA). Examples of thermograms for hybrids with ~80 wt % MTM are presented in Figure 4, and degradation temperatures

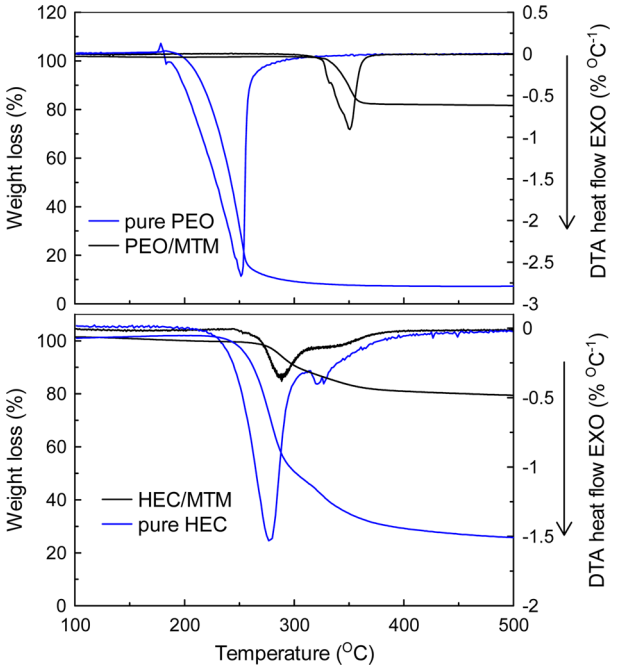

Figure 4. TGA plots showing weight loss and its derivative vs temperature for neat polymers and their hybrids with a MTM content of ~80 wt %. Downward peaks represent DTA curve.

Table 2. Temperature at the Onset of Thermal Degradation (T_{onset}) and Temperature at the Maximum Degradation Rate (T_{max}) for Neat Polymers and Their Hybrids Having ~80 wt % MTM

	PEO	PEO/MTM	HEC	HEC/MTM
T_{onset} (°C)	219	335	257	273
T_{max} (°C)	251	351	277	288

are compiled in Table 2. Pure PEO polymer has an onset degradation temperature (T_{onset}) of 219 °C which is shifted in the corresponding hybrid by 116 °C to 335 °C. Similarly, the temperature at the maximum degradation rate is shifted by 100 °C in the PEO hybrid compared to the pure PEO (see Table 2). Enhancement of heat durability of the hybrid with respect to the pure polymer has been reported elsewhere[32,40] and may be caused from the surrounding, fixation, and stabilization of PEO chains with clay platelets. The HEC/MTM hybrid shows minor improvement in thermal degradation behaviour compared to the neat HEC. The T_{onset} occurring at 257 °C for the pure HEC is delayed to 273 °C for the HEC/MTM composite. The degradation mechanisms are obviously different for the two hybrids possibly due to different distribution and interactions of their constituents.

The results from transparency, mechanical, and thermal stability suggest that the PEO interact much more strongly with MTM than HEC, and this could be due to an ordering of PEO in MTM galleries,[33] while HEC would lead to lower and less regular interactions with MTM. Furthermore, there is a change of the polymeric conformation from random coil in solution to an extended chain on clay surface, thereby creating more polymer−clay interaction.[50] These interactions on MTM-polymer interface may be favorable for PEO/MTM system.

Thermomechanical Properties. Thermomechanical properties of the hybrids and neat polymer matrices evaluated by DMTA are presented in Figure 5. The hybrids maintain a

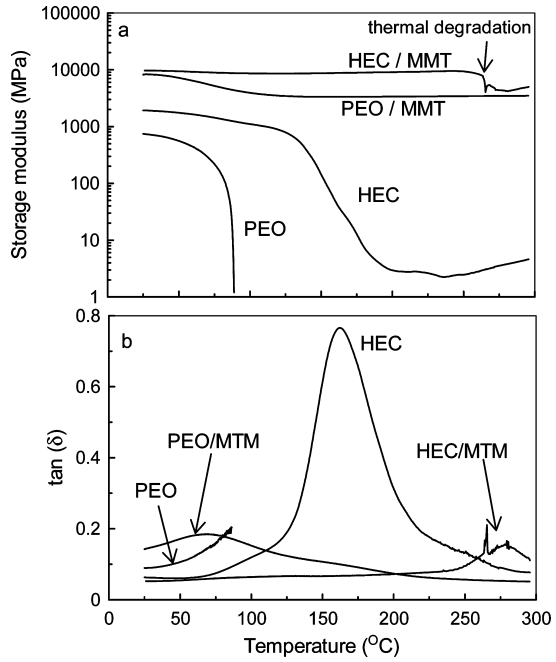

Figure 5. (a) Storage modulus and (b) tan δ as a function of temperature for neat polymers and their hybrids with 80 wt % MTM.

storage modulus above 3 GPa even at the highest temperature of 300 °C (Figure 5a). This can be attributed to the stiffness and thermal stability of MTM platelets, and to polymer intercalation and strong association with the platelets. Neat PEO and HEC polymers show strongly reduced storage moduli at 85 and 175 °C, respectively, because of melting of crystalline regions of PEO and glass transition of HEC, respectively. Note that at the end of the DMA test, the PEO/MTM hybrid did not show any discolouration or other exterior sign of thermal degradation since its degradation temperature is above 300 °C. In contrast, HEC hybrid underwent severe thermal degradation and is brownish at the end of the test as thermal degradation around 265 °C occurred. This is marked by a sudden drop in the storage modulus from 9 to 5 GPa because of a poor contribution of the HEC matrix to the hybrid mechanical performance above 265 °C. In terms of mechanical performance at high temperature, these data confirm superiority of high nanoclay content hybrids to their lower content conterparts. These latters have a storage modulus far below 1 GPa at elevated temperatures.[41,42] Nanostructured composites with high reinforcement content are therefore interesting for their thermomechanical properties.[38,43] The tangent delta curve shows a strong damping reduction of the HEC hybrid compared to the neat matrix, due to low content of HEC matrix and to reduction of polymer mobility near the MTM surface (Figure 5b).

Moisture Uptake. We further investigated performance of the hybrids in moist conditions. Moisture uptake data are presented in Figure 6a. The low moisture uptake of the hybrids

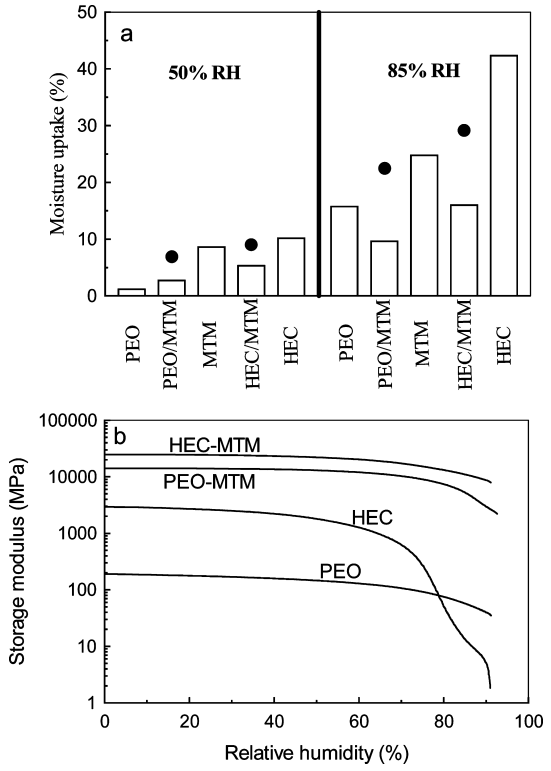

Figure 6. (a) Moisture uptake at 50% and 85% relative humidity of neat polymers and their hybrids with 75 wt % MTM, black circles correspond to a theoretical moisture uptake assuming the rule of mixture. (b) Storage modulus as a function of relative humidity for neat polymers and their hybrids with 75 wt % MTM.

with respect to the high moisture uptake of its constituents is remarkable. Black circles in Figure 6a show the theoretical moisture uptake when the rule of mixture (series model) is applied. The series model may be used as a tool for estimating composites properties.[44] It is apparent that the hybrid adsorbs much less moisture compared to the sum of its individual constituents' moisture uptake. Hence, the MTM and polymer component are individually hydrophilic and uptake a large amount of water. In the hybrid however, the interaction of the hydrophilic clay surface with the polymer reduces the hydrophilicity of the hybrid. Since the present hybrids are structured in the nanometer scale, the intercalation of polymer between MTM platelets maximizes the surface area of interaction between the organic and inorganic constituents resulting in lower adsorption of water molecules into the hybrid. These interactions are favored even in moist conditions.

Hygromechanical Properties. Hygromechanical properties of the hybrids have been measured (fig. 6b). Equilibrium storage moduli in the dry state (0% RH) are 15 GPa and 25 GPa for PEO and HEC hybrids respectively. The low moisture uptake of the hybrids results in their excellent mechanical performance in the whole humidity range studied (0-94% RH). At the humidity rate of 1% RH min^{-1}, the storage modulus of the hybrids is above 10 GPa up to 70% and 87% RH for the PEO and HEC hybrids, respectively, although effects from the lower permeability of the hybrids might contribute to the high mechanical properties observed. Equilibrium storage moduli at 94% RH ($E'_{94\%}$) are 2 and 2.7 GPa for the PEO and HEC hybrids respectively, and that is significant at such high humidity conditions where the pure polymers lose significantly their mechanical stiffness ($E'_{94\%}$ for the pure matrices is below 10 MPa).

Flame Retardant Behavior. Flame retardant behavior of PEO hybrid has been investigated by exposing a 35 μm thick film with 75 wt % inorganic content to a high temperature flame (see Video 1). During the first second of contact between the film and the flame, the hybrid seems to undergo a melting of the PEO matrix. This is followed by a short and blazing burning of the organic component (Figure 7, 1 s) succeeded by

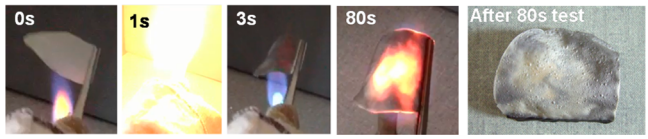

Figure 7. Photographs showing behaviour of PEO/MTM hybrid in presence of a high temperature flame. Top left represents the contact time between the flame and the hybrid. Also see Video 1.

self-extinguishing of the hybrid (Figure 7, 3 s). The delayed burning of the matrix would be due to a tortuous diffusion path for oxygen and volatiles throughout the film, and is different from what has been reported for a chitosan/MTM hybrid,[23] whose burning is immediate. Subsequently, the film loses its flexibility but maintains its shape and integrity and behaves as a fire-shielding ceramic (Figure 7; 80 s). The films remained impermeable to the flame during the 80 second of the test. The observations regarding flame retardant behavior were also observed in substrates coated with clay–polymer using LbL technique.[6,7]

Oxygen and Water Vapor Barrier Properties. To illustrate property advantages due to hybrid layered structure parallel to the film surface, barrier properties of the hybrids against oxygen and water vapor have been investigated. Results are shown in Table 3. While neat polymer matrices have poor

Table 3. Oxygen Permeability in [cc mm m^{-2} day^{-1} atm^{-1}] (OP) and Water Vapor Permeability in [10^6 (g/day m Pa)] (WVP)[a]

	OP at 50%	OP at 80%	WVP at 50%	WVP at 85%
PEO	n.a	*b*	*c*	*c*
HEC	n.a	226	23.8	74.3
PEO/MTM	0.06[d]	0.29[e]	0.26[g]	0.54[i]
HEC/MTM	0.14[e]	0.20[f]	0.47[h]	4.3[i]

[a]n.a means not available. [b]OTR higher than the upper limit measurable with Systech that is 432000 cc m^{-2} day^{-1}. [c]Steady state was not achievable. [d]MTM weight % in the hybrid is 71. [e]MTM weight % in the hybrid is 85. [f]MTM weight % in the hybrid is 60. [g]MTM weight % in the hybrid is 77. [h]MTM weight % in the hybrid is 72. [i]MTM weight % in the hybrid is 75.

barrier performance, introduction of impermeable clay platelets into the films generates a labyrinth within the structure that significantly delays passage of oxygen and water molecules through the sample. This results in a significantly lowered permeability of the hybrids, that is ~2 orders of magnitude lower than permeability of pure matrices. At 50% RH, the lowest O_2 permeability (OP; see unit in Table 3 legend) data observed for the PEO/MTM hybrid is comparable to OP for cellulose nanofibers/MTM hybrids (OP of 0.045),[25] but lower than OP for negatively charged cellulose nanofibers/MTM hybrids (OP of 0.007 and 0.004).[28,45] This is due to the

excellent barrier performance of cellulosic nanofibers at ambient humidity forming a tight network hindering passage of oxygen molecules. Hybrids based on cellulosic nanofibers however, show a relatively high OP at high humidity atmospheres. 20 and 80 folds increase in the OP were reported for cellulosic nanofiber hybrids when the humidity rose from 50% RH to 80% or 95% RH, respectively.[25,28] The OP of the present hybrids seems to be much less affected by the relative humidity increase, most probably due to their low moisture uptake also at elevated humidity conditions. At 80% RH, OP of the present hybrid compares to the best O_2 barrier hybrids reported in the literature (0.325 for PVA/MTM,[7] 0.15 for cellulose nanofibers/MTM,[13] and 0.15 for hemicellulose/MTM[46]). For indication, the best barrier polymer, that is, EVOH, has an OP of ~0.05 at 80% RH.[47]

Water vapor permeability (WVP; see unit in Table 3 legend) of the PEO hybrid at 85% RH is particularly low, lower than what has been reported for cellulose nanofibers/clay hybrids (WVP of 1.83 and 2.2 at 80% and 85% RH, respectively).[28,48] Combination of low OP and WVP of the present hybrids is exceptional. Additional advantages such as flexibility and optical translucency makes the present hybrids of possible interest in packaging or electronic display applications.

CONCLUSIONS

A paper-making filtering route was used to assemble Montmorillonite platelets and a water-soluble polymer into films of high inorganic content (60−85 wt %). Hybrids having an in-plane layered structure with polymer intercalating MTM galleries resulted. These hybrids exhibit a high degree of flexibility despite the brittle nature of their main ceramic constituent, and this has been attributed to the interlayer plastic deformation of the polymer and its soft interfacial interactions with the platelets. The remarkable tensile strain-to-failure of the hybrids in the range 2.7−8.6% with a distinct plastic deformation zone supports this observation. The high strain to failure of the present hybrids, combined with a fairly good strength makes them amongst the toughest hybrids reported with similar inorganic content. The PEO/MTM hybrid exhibits a delayed thermal degradation of the polymer matrix by 100 °C because of polymer stabilization by MTM and favorable interactions between the components. Moreover, the present hybrids displayed a low moisture uptake, much lower than what is predicted by the rule of mixture. Clearly, nanostructured hybrids are not only the sum of their primary components but a large synergy effect results from the nanoscale polymer intercalation and interactions with the platelets. These interactions are maintained at high temperature and in moist conditions conferring the hybrids with a significant storage modulus above 2 GPa at 300°C or 94% RH. The hybrid is also fire retardant and displays good barrier performance against oxygen and water vapor even under high humidity. Well aligned platelets parallel to the film surface would have a major contribution to flame retardancy and low permeability performances of the hybrids. The green and scalable processing route, combined with high toughness, thermal, and barrier performances of the present hybrids may promote their usage in packaging, transportation, construction, and insulation applications.

ASSOCIATED CONTENT

Supporting Information

High resolution FE-SEM of tensile fractured cross-section of PEO/MTM hybrid. This material is available free of charge via the Internet at http://pubs.acs.org.

Web-Enhanced Feature

Video showing fire shielding property of PEO/MTM hybrid with 75 wt % MTM content.

AUTHOR INFORMATION

Corresponding Author

*Tel.: +41587656118. E-mail: houssine.sehaqui@empa.ch.

Notes

The authors declare no competing financial interest.

ACKNOWLEDGMENTS

The SSF Fire Foam Center is acknowledged for partial funding of J.K. Dr Sebastien Josset from EMPA is thanked for assistance in performing anti-flammability test. Mr Roland Lüscher from the Multimedia center at EMPA is thanked for assistance in video file conversion. Mr Hamza Sehaqui is thanked for designing graphical entry.

REFERENCES

(1) Sanchez, C.; Julian, B.; Belleville, P.; Popall, M. *J. Mater. Chem.* **2005**, *15*, 3559−3592.
(2) Liu, L. M.; Qi, Z. N.; Zhu, X. G. *J. Appl. Polym. Sci.* **1999**, *71*, 1133−1138.
(3) Kojima, Y.; Usuki, A.; Kawasumi, M.; Okada, A.; Fukushima, Y.; Kurauchi, T.; Kamigaito, O. *J. Mater. Res.* **1993**, *8*, 1185−1189.
(4) Boesel, L. F.; de Geus, M.; Thony-Meyer, L. *J. Appl. Polym. Sci.* **2013**, *129*, 1109−1116.
(5) Gilman, J. W. *Appl. Clay Sci.* **1999**, *15* (1-2), 31−49.
(6) Laufer, G.; Kirkland, C.; Cain, A. A.; Grunlan, J. C. *ACS Appl. Mater. Inter.* **2012**, *4*, 1643−1649.
(7) Li, Y.-C.; Schulz, J.; Mannen, S.; Delhom, C.; Condon, B.; Chang, S.; Zammarano, M.; Grunlan, J. C. *ACS Nano* **2010**, *4*, 3325−3337.
(8) Yano, K.; Usuki, A.; Okada, A.; Kurauchi, T.; Kamigaito, O. *J. Polym. Sci., Part A: Polym. Chem.* **1993**, *31*, 2493−2498.
(9) Messersmith, P. B.; Giannelis, E. P. *J. Polym. Sci., Part A: Polym. Chem.* **1995**, *33*, 1047−1057.
(10) Gorrasi, G.; Tortora, M.; Vittoria, V.; Pollet, E.; Lepoittevin, B.; Alexandre, M.; Dubois, P. *Polymer* **2003**, *44*, 2271−2279.
(11) Tsai, T. Y.; Li, C. H.; Chang, C. H.; Cheng, W. H.; Hwang, C. L.; Wu, R. J. *Adv. Mater.* **2005**, *17*, 1769−1773.
(12) Alexandre, M.; Dubois, P. *Mater. Sci. Eng. Res.* **2000**, *28*, 1−63.
(13) Ray, S. S.; Bousmina, M. *Prog. Mater. Sci.* **2005**, *50*, 962−1079.
(14) Ray, S. S.; Okamoto, M. *Prog. Polym. Sci.* **2003**, *28*, 1539−1641.
(15) Meyers, M. A.; Chen, P. Y.; Lin, A. Y. M.; Seki, Y. *Prog. Mater. Sci.* **2008**, *53*, 1−206.
(16) Podsiadlo, P.; Kaushik, A. K.; Arruda, E. M.; Waas, A. M.; Shim, B. S.; Xu, J. D.; Nandivada, H.; Pumplin, B. G.; Lahann, J.; Ramamoorthy, A.; Kotov, N. A. *Science* **2007**, *318*, 80−83.
(17) Svagan, A. J.; Akesson, A.; Cardenas, M.; Bulut, S.; Knudsen, J. C.; Risbo, J.; Plackett, D. *Biomacromolecules* **2012**, *13*, 397−405.
(18) Kleinfeld, E. R.; Ferguson, G. S. *Science* **1994**, *265*, 370−373.
(19) Decher, G. *Science* **1997**, *277*, 1232−1237.
(20) Deville, S.; Saiz, E.; Nalla, R. K.; Tomsia, A. P. *Science* **2006**, *311*, 515−518.
(21) Munch, E.; Launey, M. E.; Alsem, D. H.; Saiz, E.; Tomsia, A. P.; Ritchie, R. O. *Science* **2008**, *322*, 1516−1520.
(22) Walther, A.; Bjurhager, I.; Malho, J. M.; Pere, J.; Berglund, L.; Ikkala, O. *NanoLetters* **2010**, *10*, 2742−2748.
(23) Yao, H.-B.; Tan, Z.-H.; Fang, H.-Y.; Yu, S.-H. *Angew. Chem., Int. Ed.* **2010**, *49*, 10127−10131.

(24) Priolo, M. A.; Gamboa, D.; Holder, K. M.; Grunlan, J. C. *Nano Lett.* **2010**, *10*, 4970−4974.
(25) Liu, A.; Walther, A.; Ikkala, O.; Belova, L.; Berglund, L. A. *Biomacromolecules* **2011**, *12*, 633−641.
(26) Sehaqui, H.; Liu, A. D.; Zhou, Q.; Berglund, L. A. *Biomacromolecules* **2010**, *11*, 2195−2198.
(27) Kochumalayil, J. J.; Bergenstrahle-Wohlert, M.; Utsel, S.; Wagberg, L.; Zhou, Q.; Berglund, L. A. *Biomacromolecules* **2013**, *14*, 84−91.
(28) Aulin, C.; Salazar-Alvarez, G.; Lindstrom, T. *Nanoscale* **2012**, *4*, 6622−6628.
(29) Henriksson, M.; Berglund, L. A.; Isaksson, P.; Lindstrom, T.; Nishino, T. *Biomacromolecules* **2008**, *9*, 1579−1585.
(30) Kerekes, R. J.; Schell, C. J. *Tappi J.* **1995**, *78*, 133−139.
(31) Giannelis, E. P. *Adv. Mater.* **1996**, *8*, 29−35.
(32) Wu, J. H.; Lerner, M. M. *Chem. Mater.* **1993**, *5*, 835−838.
(33) Ruizhitzky, E.; Aranda, P. *Adv. Mater.* **1990**, *2*, 545−547.
(34) Dundigalla, A.; Lin-Gibson, S.; Ferreiro, V.; Malwitz, M. M.; Schmidt, G. *Macromol. Rapid Commun.* **2005**, *26*, 143−149.
(35) Liu, A.; Berglund, L. A. *Eur. Polym. J.* **2013**, *49*, 940−949.
(36) Das, P.; Schipmann, S.; Malho, J.-M.; Zhu, B.; Klemradt, U.; Walther, A. *ACS Appl. Mater. Inter.* **2013**.
(37) Walther, A.; Bjurhager, I.; Malho, J. M.; Ruokolainen, J.; Berglund, L.; Ikkala, O. *Angew. Chem., Int. Ed.* **2010**, *49*, 6448−6453.
(38) Sehaqui, H.; Zhou, Q.; Berglund, L. A. *Soft Matter* **2011**, *7*, 7342−7350.
(39) Sehaqui, H.; Morimune, S.; Nishino, T.; Berglund, L. A. *Biomacromolecules* **2012**, *13*, 3661−3667.
(40) Burgaz, E. *Polymer* **2011**, *52*, 5118−5126.
(41) Ogata, N.; Kawakage, S.; Ogihara, T. *J. Appl. Polym. Sci.* **1997**, *66*, 573−581.
(42) Ogata, N.; Kawakage, S.; Ogihara, T. *Polymer* **1997**, *38*, 5115−5118.
(43) Boujemaoui, A.; Carlsson, L.; Malmstrom, E.; Lahcini, M.; Berglund, L.; Sehaqui, H.; Carlmark, A. *ACS Appl. Mater. Inter.* **2012**, *4*, 3191−3198.
(44) Luo, J.-J.; Daniel, I. M. *Compos. Sci. Technol.* **2003**, *63*, 1607−1616.
(45) Wu, C. N.; Saito, T.; Fujisawa, S.; Fukuzumi, H.; Isogai, A. *Biomacromolecules* **2012**, *13*, 1927−1932.
(46) Yaich, A. I.; Edlund, U.; Albertsson, A.-C. *Carbohydr. Polym.* **2013**, in press.
(47) Lagaron, J. M.; Cabedo, L.; Cava, D.; Feijoo, J. L.; Gavara, R.; Gimenez, E. *Food Addit. Contam.* **2005**, *22*, 994−998.
(48) Ho, T. T. T.; Zimmermann, T.; Ohr, S.; Caseri, W. R. *ACS Appl. Mater. Inter.* **2012**, *4*, 4832−4840.
(49) Bonderer, L. J.; Studart, A. R.; Gauckler, L. J. *Science* **2008**, *319*, 1069−1073.
(50) Theng, B. K. G. *Clay Clay Miner.* **1982**, *30*, 1−10.